Impact of stochastic ocean density corrections on air-sea flux variability

Niraj Agarwal[1], R. Justin Small[3], Frank O. Bryan[3], Ian Grooms[2], Philip J. Pegion[4]

[1] University of Colorado Boulder/CIRES, Boulder, CO, USA

[2] Department of Applied Mathematics, University of Colorado Boulder, Boulder, CO, USA

[3] Climate and Global Dynamics Laboratory, National Center for Atmospheric Research, Boulder, CO, USA

[4] NOAA Physics Sciences Division, Boulder, CO, USA

Contents of this file

Introduction

Below we have provided a set of supplementary figures with short explanations for a better understanding of the manuscript.
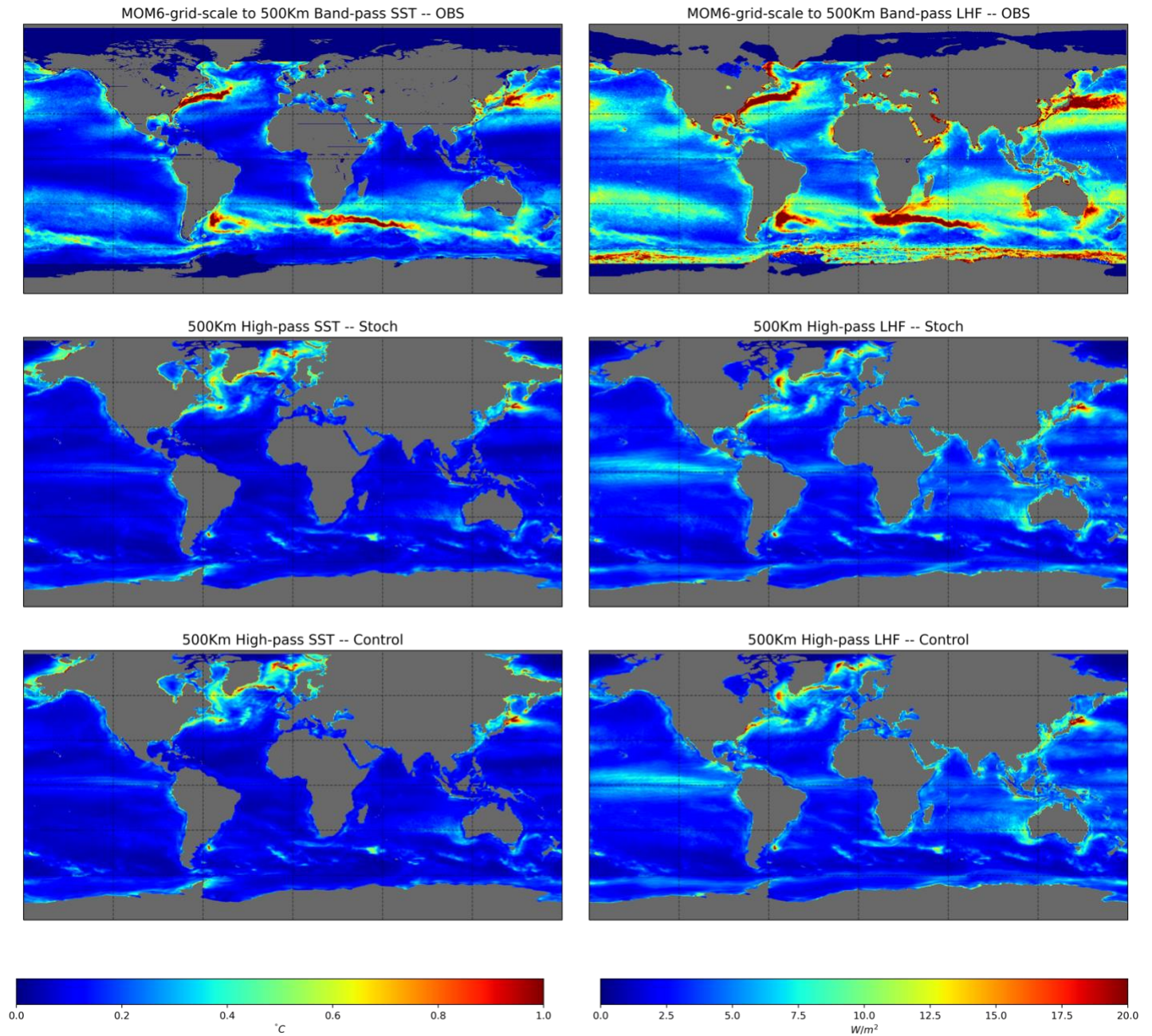
Figure S1. A comparison of the standard deviation of high-pass SST (left column) and LHF (right column) from OBS (top row), Stoch (middle row), and Control (bottom row) for 500 km filter scale. OBS is band-pass filtered to retain the scales between the MOM6 grid size and 500 km. MOM6 simulations (both Stoch and Control) lack a significant proportion of the high-frequency variability inherent to mesoscale eddies along the boundary currents compared to the OBS.
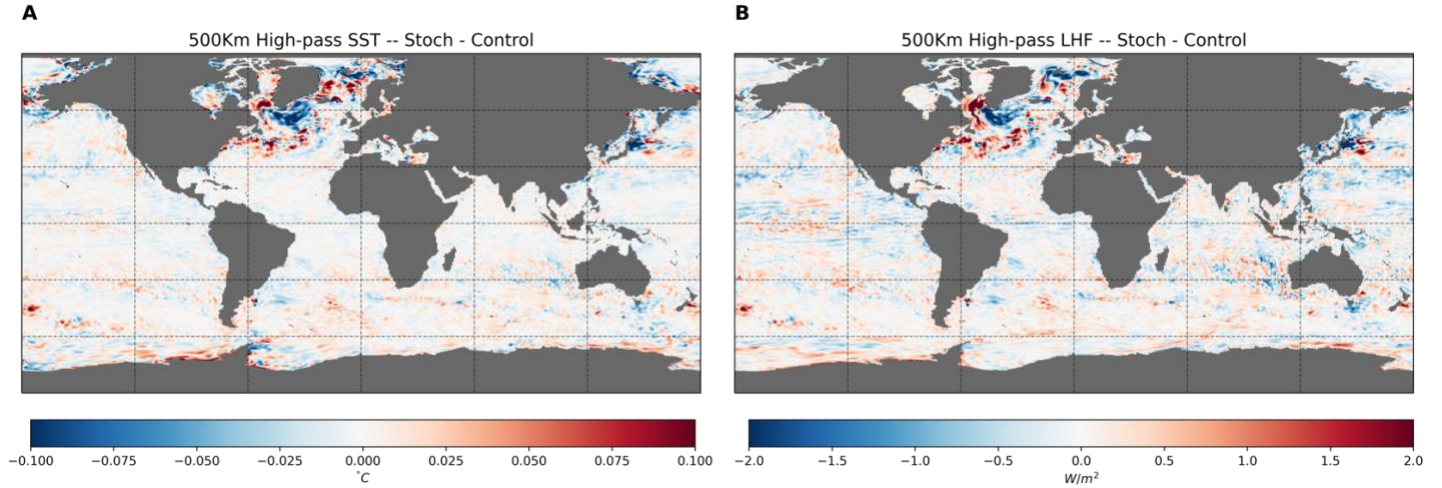
A   500Km High-pass SST -- Stoch - Control   **B**   500Km High-pass LHF -- Stoch - Control

Figure S2. (a) Difference in the standard deviation of high-pass SST from Stoch and Control simulations for 500 km filter size; (b) same as (a) but for LHF. Note: this figure is essentially the subtraction of bottom row from the middle row in Fig. S1. The most notable changes are present along the Labrador and Irminger seas, which are strongly correlated to the changes in the wintertime mixed layer depths in these regions. Furthermore, both panels exhibit almost the same pattern, inferring that the SST anomalies (i.e., oceans) force the THF variability (or atmosphere) at mesoscales.
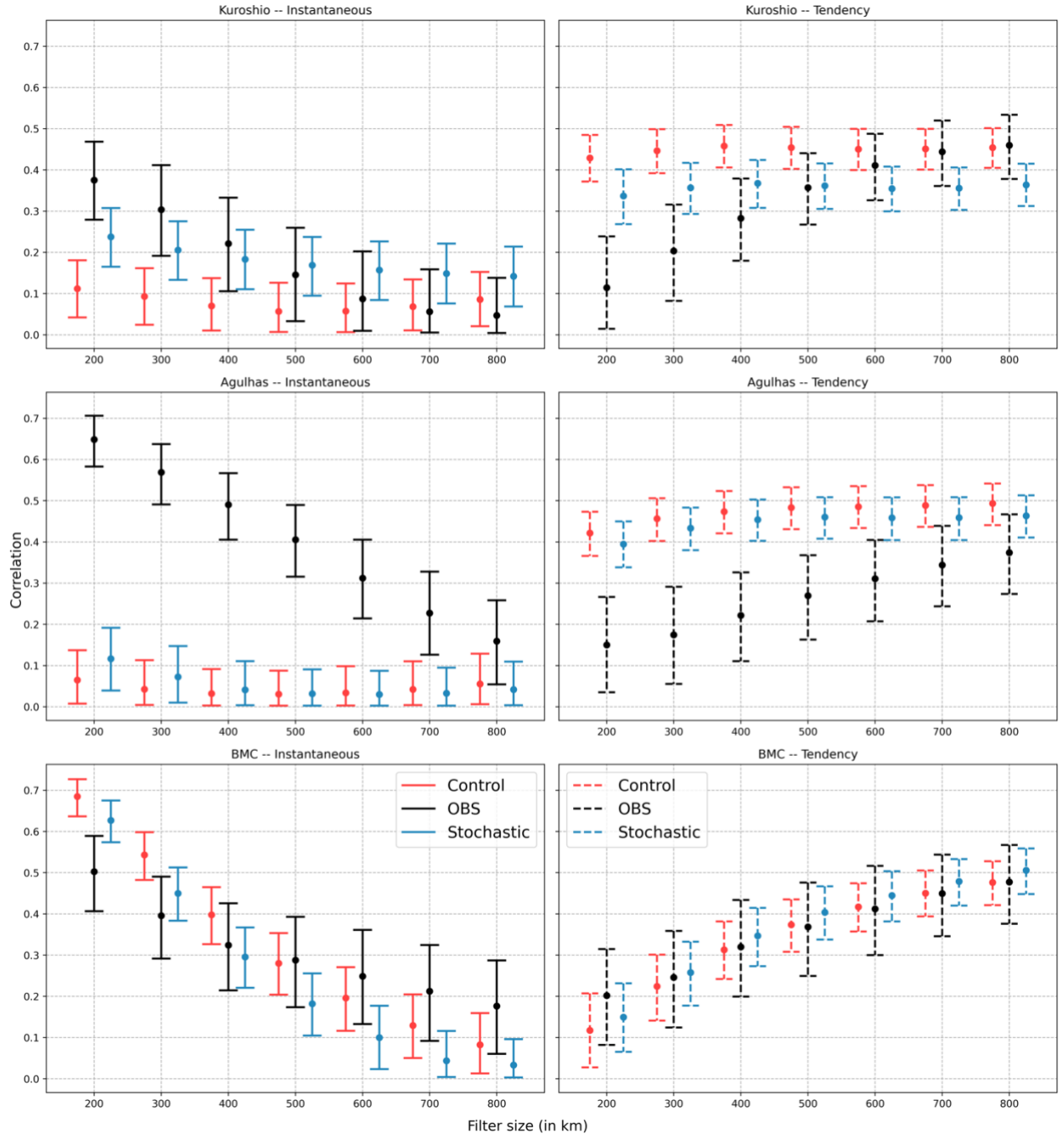
Figure S3. Plots of 95% confidence interval (CI) for SST-LHF (left column) and $\partial(SST)/\partial t$-LHF (right column) correlation using the low-pass components from various filter sizes. These belong to the Kuroshio, Agulhas, and BMC locations (top to bottom) marked by green stars in Fig. 2 in the main text. In general, Stoch CIs are closer to OBS than Control for filter sizes up to 500 km. The Agulhas location is an exception, as it lacks a large extent of SST-LHF covariability for both Stoch and Control compared to the OBS. An enhanced SST-LHF correlation for

Stoch proves that we are augmenting SST-LHF feedback inherent to mesoscale eddies, which the stochastic density parameterization focuses on.
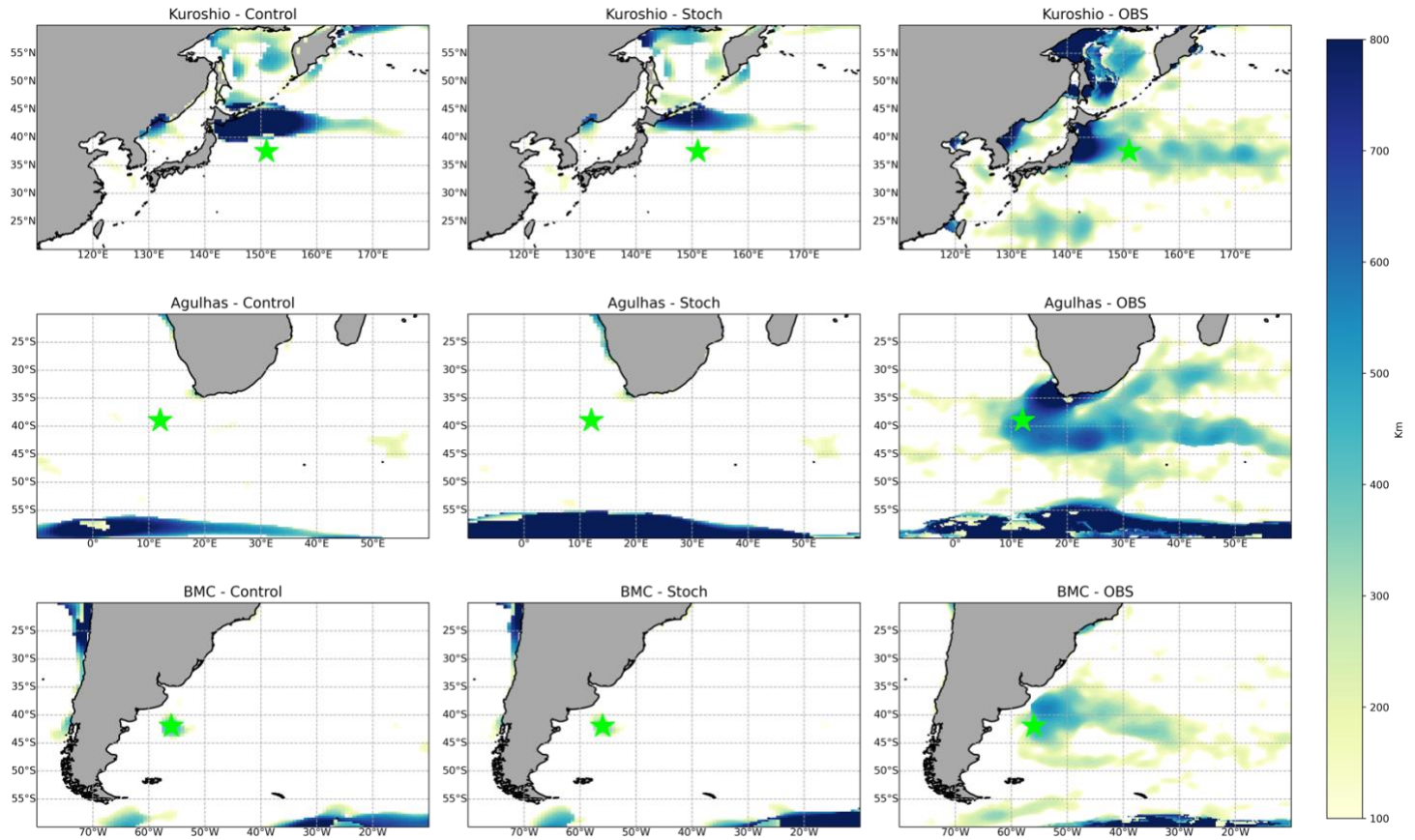

Figure S4. Spatial maps of the transition length scale for Kuroshio, Agulhas, and BMC regions (top to bottom) for Control, Stoch, and OBS (left to right). In the Kuroshio region (top row), subtle differences between Stoch and Control exist about east of Japan, but the Kuroshio extension is shifted far north in both Control and Stoch compared to the OBS. This is why we do not study these differences further. The Stoch and Control outputs are nearly identical in the Agulhas and BMC regions except for minor changes in the magnitude of the transition scales resolved in the two experiments. There are also changes around the Antarctic Circumpolar Current (ACC) boundary, i.e., between 55° − 60° S, but this is not an area of focus in this study.
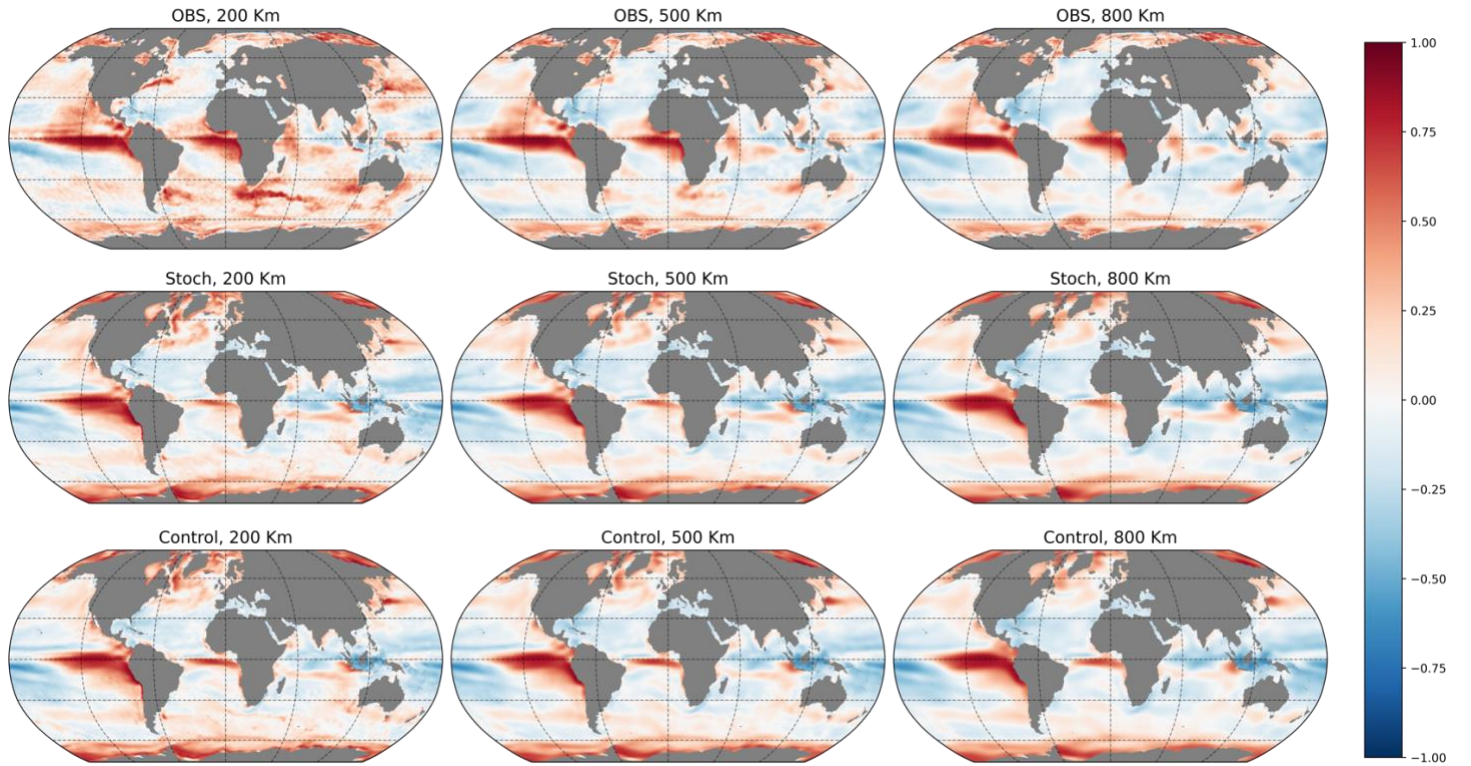
Figure S5. Global maps of the instantaneous SST-LHF correlation for low-pass SST and LHF from 200 km (left column), 500 km (middle column), and 800 km (right column) filter scales; the three rows belong to OBS (top), Stoch (middle), and Control (bottom). Coherent spatial patterns of positive correlations exist over high SST/THF variability regions, e.g., Gulf Stream, Kuroshio, and Agulhas. Because the instantaneous SST-LHF correlations quantify the oceans-forcing-atmosphere case -- inherent to small-scale oceanic eddies, we witness a general decrease in the correlations in these regions as we move from low to high filter scales. This is clearer in the panels for OBS. The strong correlations in the tropical Pacific are due to the ENSO effects.
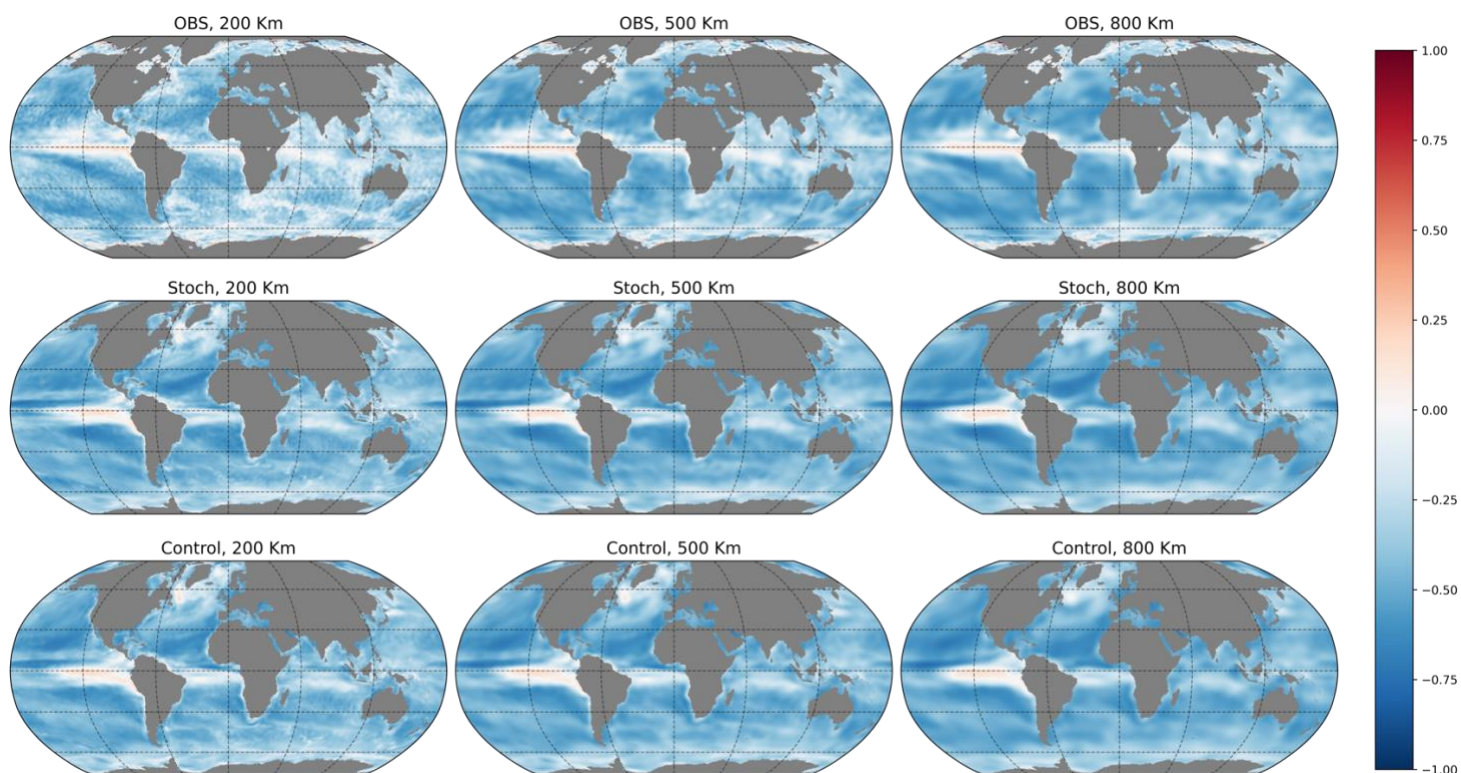
Figure S6. Same as S5 but for $\partial(SST)/\partial t$ - LHF correlation. The correlation magnitude increases globally as we move from low to high filter size (i.e., left to right) because the atmosphere-forcing-oceans case holds most strongly for synoptic scales. It is worth noting that around the major boundary currents, the sign of the correlations here is opposite to those in Fig. S5. This is due to the difference in the physical processes they represent (discussed in detail in Sec. 1 in the main text.)
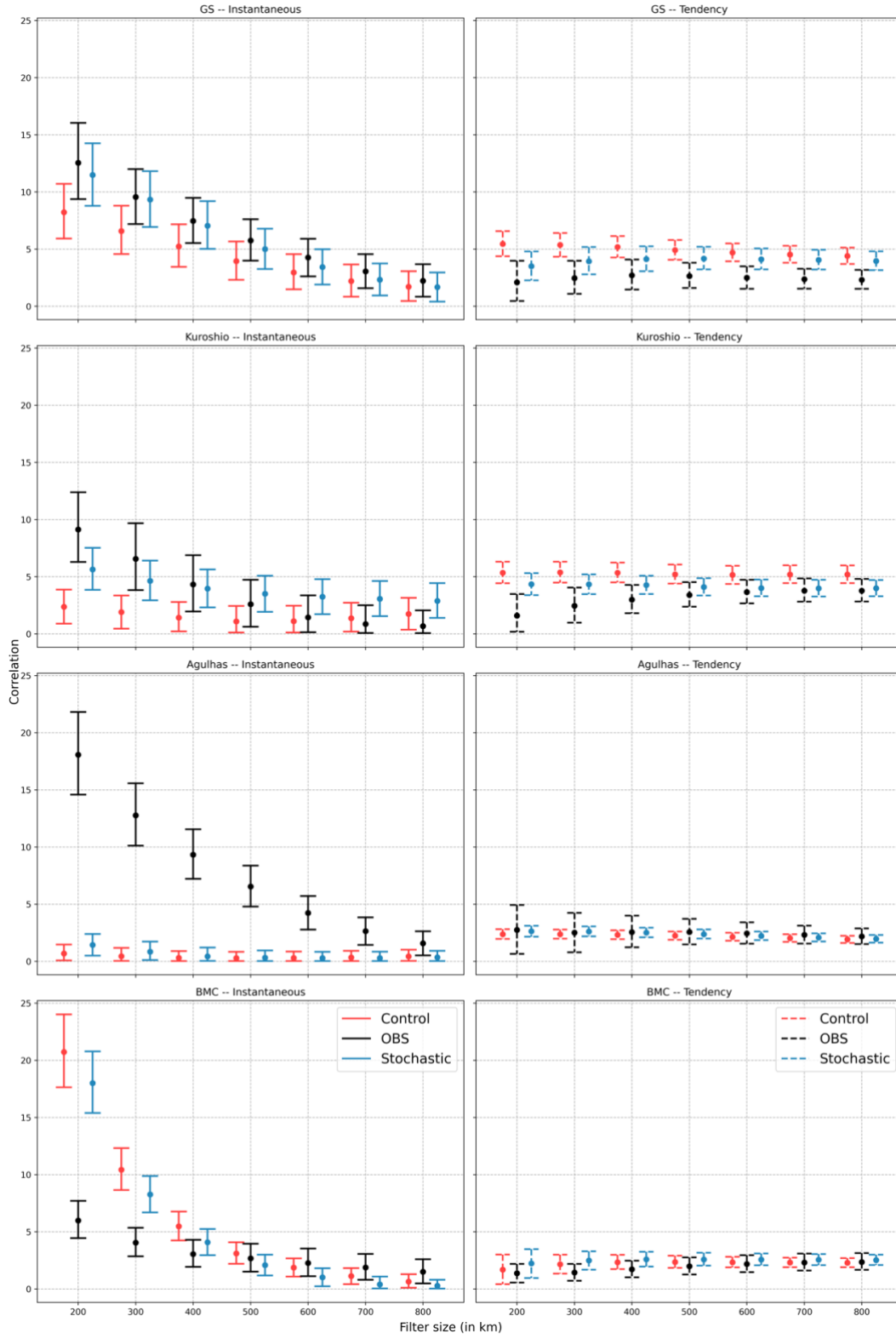
Figure S7. Same as Fig. S3 but for covariance (with an additional panel for the GS location). The GS location stands out, as the Stoch outputs (both SST-LHF and $\partial(SST)/\partial t$ -LHF covariances) are closest to the OBS in this case. The Kuroshio location also shows significant impact, but the Stoch SST-LHF covariance outputs are more

ocean-forced beyond the 400 km filter size. The Agulhas location again remains nearly insensitive to the imposed parameterization. The BMC location shows incredible improvements in the SST-LHF covariance up to 400 km filter size but underestimates it beyond this filter width. The changes in $\partial(SST)/\partial t$ - LHF covariance are marginal for all filter widths at this location.